ZESZYTY ENERGETYCZNE
TOM V. *Nowoczesne metody pomiarowe i modelowanie numeryczne w energetyce cieplnej*
2018, s. 1–13

Introduction to non-linear Thermal-FSI on the example of transient load of a thin-walled container

Bartosz Kraszewski

Institute of Fluid-Flow Machinery Polish Academy of Sciences
Energy Conversion Department
E-mail: bkraszewski@imp.gda.pl

RECOMMENDATION: *prof. dr hab. inż. Janusz Badur*

ABSTRACT

This paper presents the problems associated with the transient thermal load of structures exhibiting a non-linear relationship between load and strain. The mathematical model required to comprehensively describe the relationship between fluid and solid has been shown from different perspectives. In addition, the Newton-Raphson method has been referred to as a way of solving nonlinear equations. The article also presents the assumptions and results of numerical analysis of thin-walled container thermally loaded by contact with hot water. The conclusions drawn emphasize the importance of Thermal-FSI tools, especially in the power engineering sector.

KEYWORDS: *Thermal-FSI, CFD, CSD, non-linear mechanics.*

1. INTRODUCTION

With the temperature changes of the selected solid body and specifically its parts, deformations occur in it corresponding to the resulting temperature differences between selected elements of the structure. These deformations contribute to the thermal stresses in a given material. Uneven temperature distribution in the volume of a solid is particularly noticeable when its surface comes in contact with a selected fluid at a different temperature. The phenomena occurring in this case are subject to the analysis of the problem of thermal fluid–solid interaction (Thermal-FSI). Considering linear behavior, assuming F as an external force acting on a given solid and u as a displacement of

a material, their dependence is described in general terms by Hooke's law, by means of constant material stiffness K:

$$F = Ku \tag{1}$$

thus giving a simple relationship shown in Fig.1a.

However, non-linear behavior, occurring in most real structures is characterized by a non-linear relationship between the given force and the resulting displacement. The stiffness of the material ceases to be a constant, and becomes a force-dependent variable. The assumption of a constant stiffness of material for a non-linear structure results only in determining a straight line K^T, tangent to the course of the actual function $F(u)$, as shown in Fig. 1b.

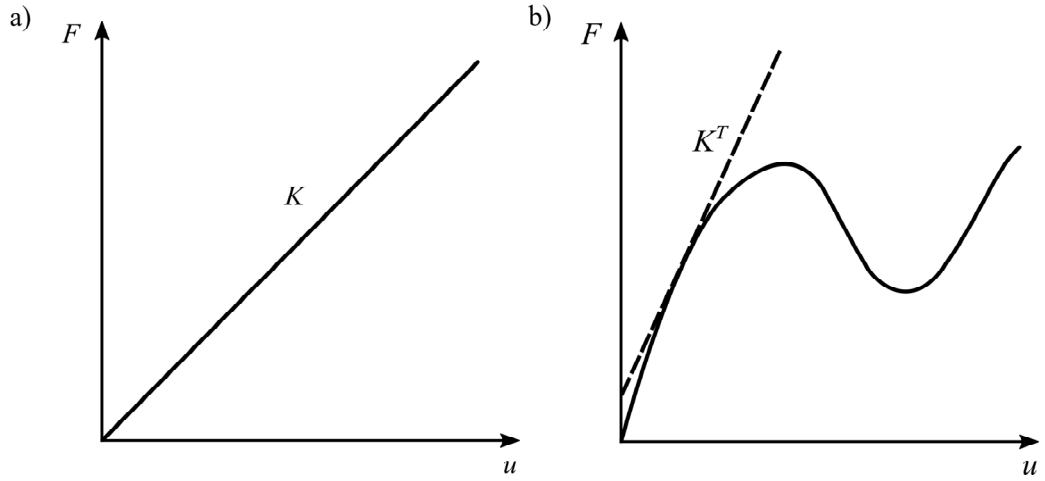

Fig. 1: Characteristics of $F(u)$: a) linear, b) non-linear

The above material bahavior is an example of one of three types of nonlinearity, where:

- mathematical nonlinearity results from the phenomenon of non-linear elements occurring in the mathematical description,
- physical (material) nonlinearity is caused by the lack of proportionality between the stress and the deformation of the material,
- geometric nonlinearity results from the lack of proportionality between strains and generalized displacements, which is particularly characteristic of flaccid structures [14].

Thus, the situation becomes more complicated when, apart from the external force, there also occur elastic forces resulting for example from the body shape (structure) and its supports as well as the effects of thermal expansion of the solid body, i.e. deformations and thermal stresses. An example of the behavior of an object subjected to such loads can be a kitchen sink made of stainless steel–in the case of contact of the sink surface with boiling water it can be heard a distinctive sound, resulting from the bulging of the sink bottom under the influence of thermal load and the elastic action of its side walls. The above-mentioned kitchen metaphor marks the presence of the non-linear Thermal-FSI phenomenon in everyday life. Thus, it should be looked at on a larger scale, particular in the professional power industry, where both temperature changes and forces are multiplied - first of all, reference should be made here to the bodies and rotors of turbines subjected to variable thermal loads. The aim of the paper is to present the non-linear Thermal-FSI phenomena on the example of numerical analysis of

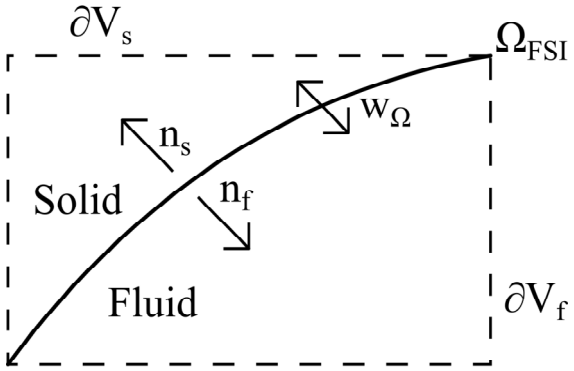

Fig. 2: Fluid–solid mid-surface

a physical object similar to the aforementioned kitchen sink-a thin-walled stainless steel container for which hot water has been poured.

2. Mathematical model

Assuming the situation in which the fluid comes into contact with a solid, there can be defined the contact surface Ω_{FSI}, its speed of movement $\mathbf{w}_\Omega$, instantaneous volumes of liquid and solid ∂V_F, ∂V_S and also normal vectors to the surface $\mathbf{n}_F$, $\mathbf{n}_S$ [6, 7, 9, 18], as shown in Fig. 2. The contact surface represents all bounary parameters. In addition, the following relationships are met [18]:

$$\mathbf{w}_\Omega = \mathbf{w}_{\text{Fluid}} = \mathbf{w}_{\text{Solid}}, \tag{2}$$

$$\mathbf{n}_F = -\mathbf{n}_S. \tag{3}$$

In the terms of numerical analysis, both the fluid and solid domain must be subdivided according to Finite Element Method (FEM) or Finite Volume Methods (FVM). Indicating ρ as a density of the continuum, and $\mathbf{v}(\mathbf{x}, t)$ as the velocity vector, the total energy is described as:

$$e = u + \frac{1}{2}\mathbf{v}^2, \tag{4}$$

where u means internal unit energy. Then, specyfing p as the hydrostatic pressure, $\mathbf{I}$ as an unit tensor, $\boldsymbol{\sigma}$ as the mechanical stresses tensor, $\boldsymbol{\tau}^t$ as the molecular tensor of total viscous stresses, the total heat flux can be presented as [2]:

$$\mathbf{q}^t = \mathbf{q} + \mathbf{q}^{\text{turb}} + \mathbf{q}^{\text{rad}} + \ldots \tag{5}$$

where $\mathbf{q}$ is a molecular heat fux, $\mathbf{q}^{\text{turb}}$ is a vector of turbulent heat fluxł and $\mathbf{q}^{\text{rad}}$ is radiation heat flux. Each of elements of the discretised geometry subject to the local form of balance equations [3, 10, 20]:

$$\partial_t \mathcal{U} + \operatorname{div}(\mathcal{F}^c + \mathcal{F}^e) = \operatorname{div}\mathcal{F}^v + S. \tag{6}$$

Individual expressions appearing in Eq.(6) can be described as:

- local change in density over time of an intense variable;

$$\partial_t \mathcal{U} = \begin{Bmatrix} \partial_t \rho \\ \partial_t(\rho \mathbf{v}) \\ \partial_t(\rho e) \end{Bmatrix}, \tag{7}$$

- convection flux through surfaces limiting the volume;

$$\mathcal{F}^c = \begin{Bmatrix} \rho\mathbf{v} \\ \rho\mathbf{v}\otimes\mathbf{v} \\ \rho e\mathbf{v} \end{Bmatrix}, \tag{8}$$

- elastic flux through surfaces limiting the volume – different for fluid and solid;

$$\mathcal{F}^e_F = \begin{Bmatrix} 0 \\ p\mathbf{I} \\ p\mathbf{v_F} \end{Bmatrix}, \quad \mathcal{F}^e_S = \begin{Bmatrix} 0 \\ \boldsymbol{\sigma} \\ \boldsymbol{\sigma}\mathbf{v_S} \end{Bmatrix}. \tag{9}$$

- diffusion flux through surfaces limiting the volume;

$$\mathcal{F}^D = \begin{Bmatrix} 0 \\ \boldsymbol{\tau}^t \\ \boldsymbol{\tau}^t\mathbf{v} + \mathbf{q}^t \end{Bmatrix}, \tag{10}$$

and S is the source inside the volume.

Considering that the flow of fluxes within a fluid-solid interaction must be preserved, the following relationship must be met [18]:

$$\mathcal{F}_F = \mathcal{F}_S. \tag{11}$$

Referring to the above, there can be defined three following FSI balance equations:

- transfer of mass flux;

$$j\mathbf{n}_F = j\mathbf{n}_S, \quad j = \sum \rho_i \mathbf{v}_i, \tag{12}$$

- transfer of momentum flux;

$$(-p\mathbf{I} + \boldsymbol{\tau}^t)\cdot\mathbf{n}_F = \boldsymbol{\sigma}\mathbf{n}_S + \mathcal{M}_\Omega, \tag{13}$$

- transfer of energy flux;

$$(-p\mathbf{v}_F + \boldsymbol{\tau}^t\mathbf{v}_F + \mathbf{q}^t)\cdot\mathbf{n}_F = (\boldsymbol{\sigma}\mathbf{v_S} + \mathbf{q}^t)\cdot\mathbf{n}_S + e_\Omega, \tag{14}$$

where $\mathcal{M}_\Omega$ has been additionally taken into account as a surface tension flux and e_Ω as a surface tension energy. On the basis of Eq.(6), the following conservative equations can also be prepared separately for each continuum. For fluid, or more likely for Computational Fluid Dynamics (CFD) [2, 3, 4, 8]:

- mass preservation equation;

$$\frac{\partial\rho}{\partial t} + \operatorname{div}(\rho\mathbf{v}) = 0, \tag{15}$$

- momentum preservation equation

$$\frac{\partial}{\partial t}(\rho\mathbf{v}) + \operatorname{div}(\rho\mathbf{v}\otimes\mathbf{v} + p\mathbf{I}) = \operatorname{div}\left(\boldsymbol{\tau}^t\right) + \rho\mathbf{f}, \tag{16}$$

- energy preservation equation;

$$\frac{\partial}{\partial t}(\rho e) + \operatorname{div}(\rho e\mathbf{v} + \rho p\mathbf{v}) = \operatorname{div}\left(\boldsymbol{\tau}^t\mathbf{v} + \mathbf{q}^t\right) + \rho\mathbf{b}\cdot\mathbf{v}, \quad \mathbf{b} = -9,81\mathbf{e}_z, \tag{17}$$

where $\mathbf{b}$ is a vector of mass force.

Additionally, above equations can be complemented by three equations of evolution [3, 2, 16, 13, 19]:

- equation of evolution of a turbulent energy field $k(x,t)$:

$$\frac{\partial}{\partial t}(\rho k) + \operatorname{div}(\rho k\mathbf{v}) = \operatorname{div}\left(\mathcal{F}_k^v\right) + S_k, \tag{18}$$

- equation of evolution of a turbulent diffusion field $\varepsilon(x,t)$:

$$\frac{\partial}{\partial t}(\rho\varepsilon) + \operatorname{div}(\rho\varepsilon\mathbf{v}) = \operatorname{div}(\mathcal{F}_\varepsilon^v) + S_\varepsilon, \tag{19}$$

- equation of evolution of a vapour quality $\mathcal{X}$:

$$\frac{\partial}{\partial t}(\rho\mathcal{X}) + \operatorname{div}(\rho\mathcal{X}\mathbf{v}) = \operatorname{div}(\mathcal{F}_\mathcal{X}) + S_\mathcal{X}, \tag{20}$$

where $\mathcal{F}_\varepsilon^D$ i $\mathcal{F}_k^D$ are diffusion fluxes described by closing equations [5]:

$$\mathcal{F}_k^D = \frac{\mu + \mu_t}{\sigma_k} k\nabla, \tag{21}$$

$$\mathcal{F}_\varepsilon^D = \frac{\mu + \mu_t}{\sigma_\varepsilon} \varepsilon\nabla, \tag{22}$$

wherein μ is a molecular viscosity coefficient, μ_t is a turbulent viscosity coefficient and σ_k i σ_ε are appropriate stresses. $\mathcal{F}_\mathcal{X}$ is a vapour quality flux [16, 19] and sources S_k, S_ε and $S_\mathcal{X}$ are defined by choosen expert's equations. Analogously to CFD equations, the following equations for Computational Solid Dynamics are determined [2, 3]:

- mass preservation equation;

$$\frac{\partial}{\partial t}(\rho) + \operatorname{div}(\rho\mathbf{v}) = 0, \tag{23}$$

- momentum preservation equation;

$$\frac{\partial}{\partial t}(\rho\mathbf{v}) + \operatorname{div}(\rho\mathbf{v}\otimes\mathbf{v}) = \operatorname{div}(\boldsymbol{\sigma}) + \rho\mathbf{b}, \tag{24}$$

- energy preservation equation;

$$\frac{\partial}{\partial t}(\rho e) + \operatorname{div}(\rho e\mathbf{v}) = \operatorname{div}\left(\boldsymbol{\sigma}\mathbf{v} + \mathbf{q}^t\right) + \mathrm{S}_e, \tag{25}$$

where S_e is an energy source. Finally, it should be taken into account that modern solvers mainly use non-conservative equations, where one equation is dependent on the previous one, respectively for mass, momentum and energy [3]:

$$\frac{\partial}{\partial t}\rho + \rho \mathrm{div}\,(\mathbf{v}) = 0, \tag{26}$$

$$\rho\mathbf{a} = \mathrm{div}\,(T) + \rho\mathbf{b}, \tag{27}$$

$$\rho\frac{\partial}{\partial t}u = \mathrm{div}\,(\mathbf{q}) + \left(-p\mathbf{I} + \boldsymbol{\tau}^t\right) \cdot \mathrm{grad}\mathbf{v}, \tag{28}$$

where **a** is an acceleration. Pointing to Lagrange coordinates, Green's finite strain tensor is described as [1, 14]:

$$\varepsilon_{ij}^G = \frac{1}{2}\left[\frac{\partial u_i}{\partial a_j} + \frac{\partial u_j}{\partial a_i} + \frac{\partial u_v}{\partial a_i}\frac{\partial u_v}{\partial a_j}\right], \quad v = 1, 2, 3, \tag{29}$$

where a_i is a starting position of the point. The total deformation of the material consists of strain tensors respectively elastic, plastic and thermal:

$$\varepsilon_{ij} = \varepsilon_{ij}^s + \varepsilon_{ij}^p + \varepsilon_{ij}^T. \tag{30}$$

Elastic deformation ε_{ij}^s results from generalized Hooke's law:

$$\sigma_{ij} = C_{ijkl}\,\varepsilon_{kl}^s, \tag{31}$$

where C_{ijkl} is a constitutive matrix for a material exhibiting the isotropy of elastic properties. The plastic deformation ε_{ij}^p results from the increase in plastic deformation under the associated flow law:

$$\dot{\varepsilon}_{ij}^p = \dot{\lambda}\frac{\partial f_\sigma}{\partial \sigma_{ij}}, \tag{32}$$

where $\dot{\lambda}$ is the Lagrange multiplier, and $f(\sigma_{ij}, q)$ is a function describing the plasticity condition representing the plastic potential. The thermal deformation resulting from the change in the body volume is determined by the formula:

$$\varepsilon_{ij}^T = \alpha(T - T_0)\,\delta_{ij}, \quad \delta_{ij} = \begin{cases} 0, & \text{for } i \neq j \\ 1, & \text{for } i = j \end{cases}, \tag{33}$$

wherein $\alpha(T)$ is a linear expansion cooficient, T is the defined temperature and T_0 is a reference temperature. Solving nonlinear and transient numerical analyzes requires the use of appropriate iterative methods. In this case, the Newton-Raphson method illustrated in Fig. 3 was used. By determining the total load as **Q**, the increase of the generalized displacement as $\triangle\mathbf{u}$ and the linear stiffness matrix as $\mathbf{K}^L$, the initial displacement is obtained [12, 14, 17]:

$$\mathbf{u}_0 = \left(\mathbf{K}^L\right)^{-1}\mathbf{Q}, \tag{34}$$

On the basis of $\mathbf{u}_0$, the stiffness increase from non-linearity $\mathbf{K}_0^{NL}$ is determined, which makes it possible to obtain a total stiffness matrix:

$$\mathbf{K} = \mathbf{K}^L + \mathbf{K}_0^{NL}. \tag{35}$$

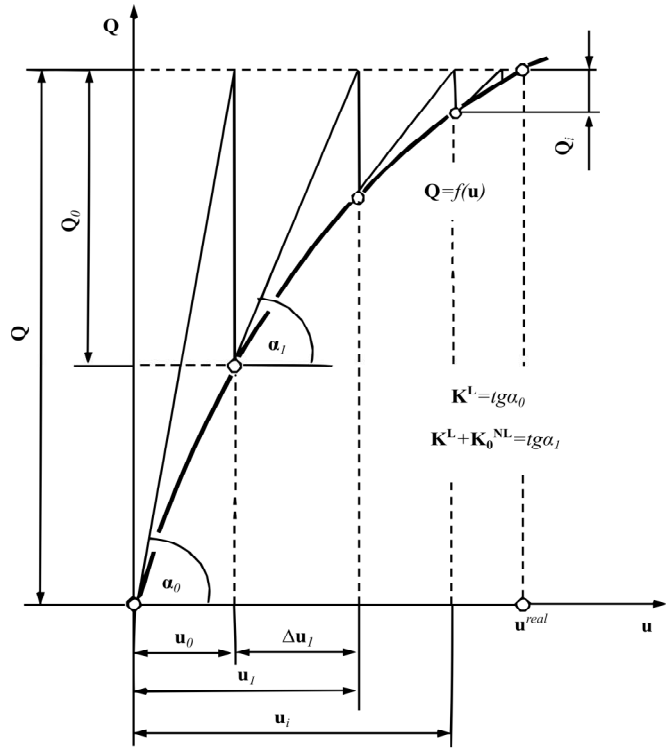

Fig. 3: One-parameter interpretation of the Newton–Raphson iterative method

The deformation state $\mathbf{u}_0$ is different from the real state, while the internal forces do not balance the load $\mathbf{Q}$, which gives an unbalanced load in the form:

$$\mathbf{Q}_0 = \left(\mathbf{K}^L + \mathbf{K}_0^{NL}\right)\mathbf{u}_0 - \mathbf{Q}, \tag{36}$$

which in turn is the source of additional displacements:

$$\triangle\mathbf{u}_1 = \left(\mathbf{K}^L + \mathbf{K}_0^{NL}\right)^{-1}\mathbf{Q}_0, \tag{37}$$

creating a new displacement state:

$$\mathbf{u}_1 = \mathbf{u}_0 + \triangle\mathbf{u}_1, \tag{38}$$

deviating from the actual state less than $\mathbf{u}_0$. This difference decreases with each i-th iteration at which $i-1$ iteration $\mathbf{u}_i$ is obtained.

3. The numerical analysis

The subject of numerical analysis of Thermal-FSI was a thin-walled stainless steel container with dimensions of 345 mm ×365 mm ×145 mm. The geometry of the thin-walled container has been discretised with a structural grid consisting of approx. 30 000 elements of 20-node type. The mesh has been properly refined at the edges, as shown in Fig. 4. In the discretization of the bottom and side walls of the structure, two layers of elements have been used.

It has been assumed that a 1.8 kg/s water stream was poured into the tank at 100°C for 1,5 s, displacing air at an ambient temperature of 20°C and at atmospheric pressure. The inlet has been specified as a 20 mm ×20 mm square. The relatively large

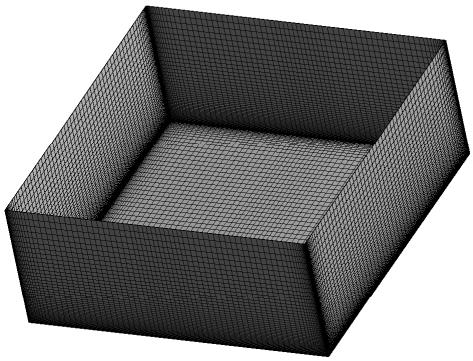

Fig. 4: Geometry of the container

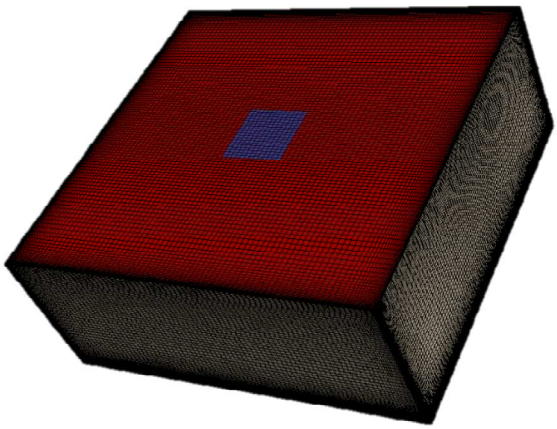

Fig. 5: The discretization of domains: blue - water inlet, red - air outlet, grey - stainless steel

flow of water enhanced the phenomena and allowed for a shorter simulation time. The structural discretisation of the fluid domain, consisting of approximately 1 million hexahedron elements, is presented in Fig. 5. The CFD analysis results are represented by the middle geometry cross-sections along the long edge. Fig. 6 and Fig. 7 show the distribution of fluids at selected times of analysis as the mass fraction of water. The results of the Thermal-FSI numerical analysis from the CFD side are presented in Fig. 8 and Fig. 9 in the form of the vertical distribution of displacement (along the Z axis) on the central cross section of the container along the long edge for characteristic time moments. Figure 10 shows the displacement of the point in the middle of the bottom of the container in time relative to the initial position for the key, first second of simulation.

4. Conclusions

The numerical analysis allowed for insight into the course of non-linear phenomena occurring during rapid contact of boiling water with a thin wall of stainless steel. The initial turn of bottom deformation is caused by the difference in temperature of elements (grains of material) in the cross-section - as the temperature is applied to the upper surface of the bottom, the heat elements expand in temperature, pushing away from the unheated lower elements of the cross-section. Then the bottom is straightened back, as a result of its complete heating and progressive thermal expansion. The final

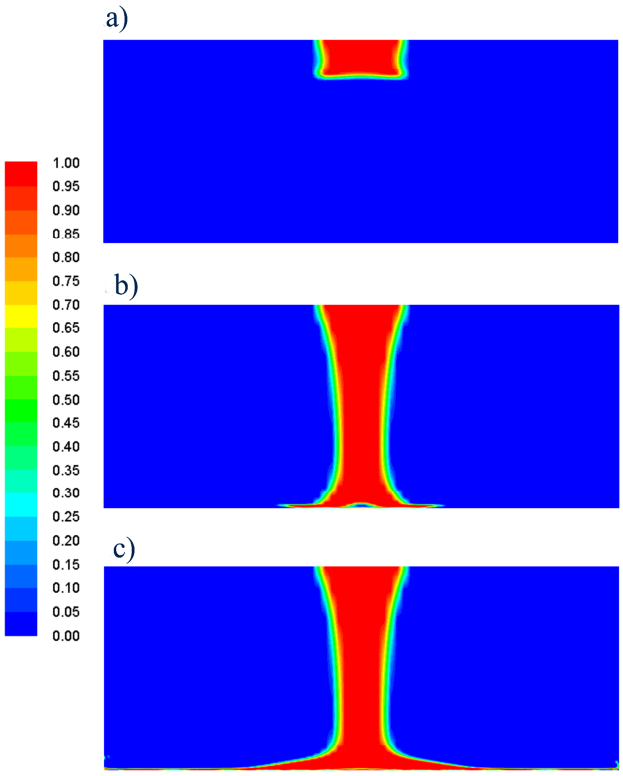

Fig. 6: Water mass fraction for simulation time: a) 0.05 s, b) 0.16 s, c) 0.19 s

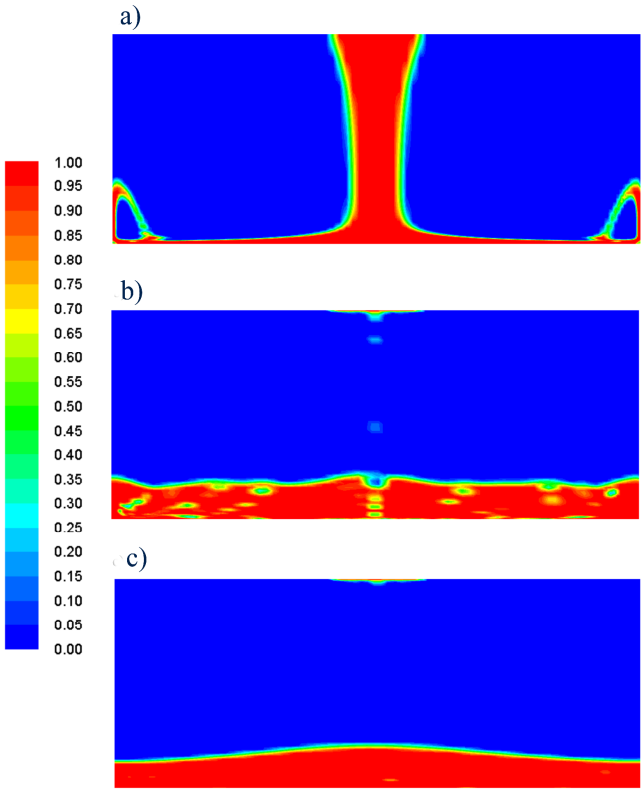

Fig. 7: Water mass fraction for simulation time: a) 0.50 s, b) 1.85 s, c) 2.95 s

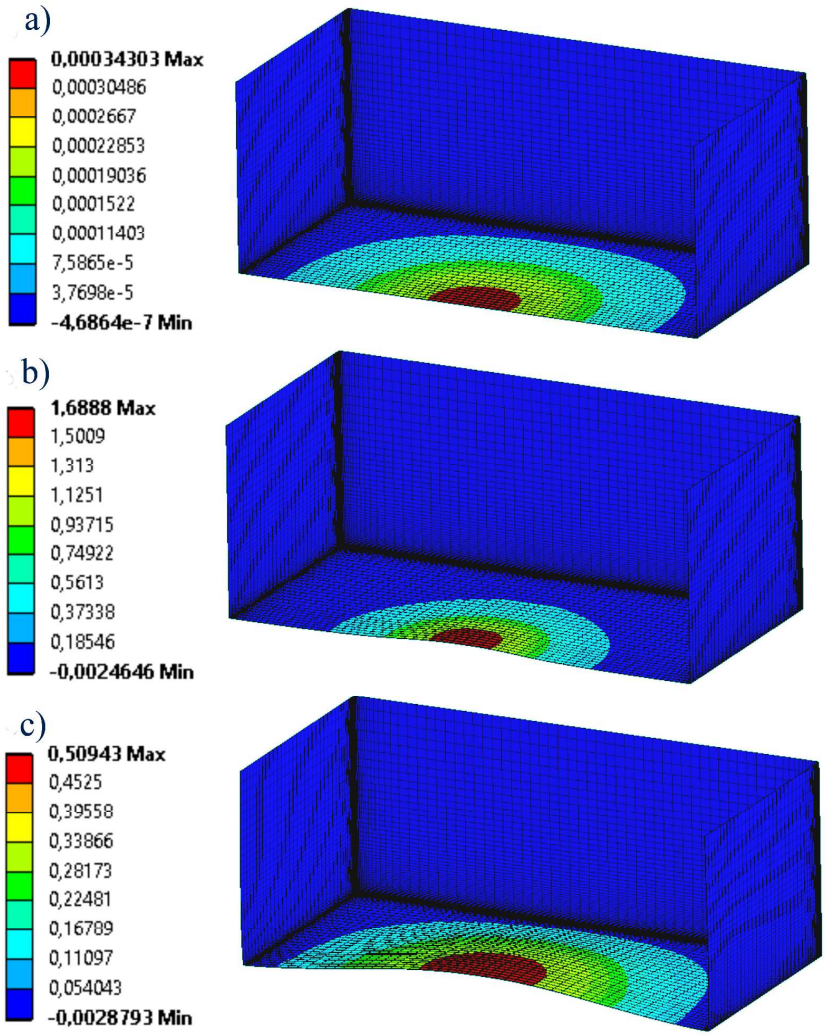

Fig. 8: Vertical displacement of the container for time: a) 0.1 s, b) 0.16 s, c) 0.19 s

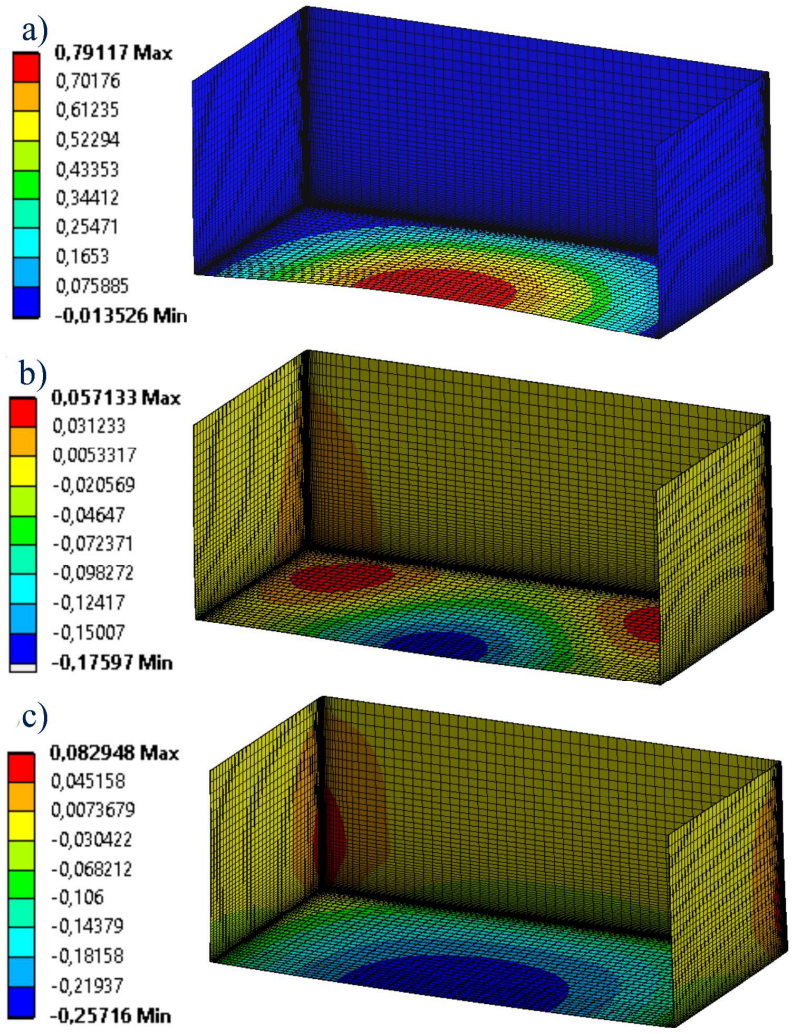

Fig. 9: Vertical displacement of the container for time: a) 0.27 s, b) 0.36 s, c) 2.95 s

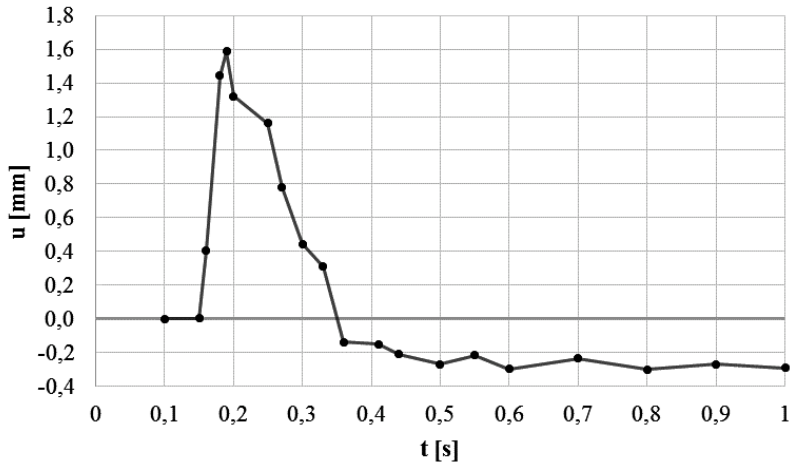

Fig. 10: A displacement at the point in the center of the upper surface of the bottom

stress caused by the pressure of the side walls to the bottom, supported by its relaxation, bends them downwards - it is these violent deflection that causes pressure disturbances in the surrounding kitchen sink air and thus the generation of an audible sound wave. This analysis demonstrates the extensive possibilities of Thermal-FSI tools that allow simulation of phenomena accompanying the interaction of fluid and solid body, as well as an in-depth insight into their course. These possibilities may turn out to be crucial in issues related to the exploitation of energy devices, thus orientating the path towards their most effective effort.

References

[1] Aravas N., *On the Numerical Integration of a Class of Pressure-Dependent Plasticity Models*, International Journal for Numerical Methods in Engineering **24** (7), 1395–1416, 1987.

[2] Badur J., *Development of the concept of energy.* IFFM PAS, Gdańsk 2009.

[3] Badur J., *Five lectures from modern fluid termomechanics.* CUT script (in Polish), www.imp.gda.pl, Gdańsk, 2002.

[4] Badur J., Bryk M., Ziółkowski P., Sławiński D., Ziółkowski P. J., Kornet S., Stajnke M., *On a comparison of Huber-Mises-Hencky with Burzynski-Pecherski equivalent stresses for glass body during nonstationary thermal load*, AIP Conference Proceedings **1822**, 2017.

[5] Badur J., Karcz M., Kucharski R., Wisniewski A. and Kekana M., *Coupled Modelling of the Cooling Processes and the Induced Thermo-Corrosive Fatigue within a Gas Turbine*,[in:] State of Art on Gas Turbine Research in Poland, Editor T. Uhl, Cracow TU Press, 19–30, 2003.

[6] Badur J., Karcz M., Lemański M., *On the mass and momentum transport in the Navier–Stokes slip layer*, Microfluid Nanofluid **11**, 439-–449, 2011.

[7] Badur J., Ziółkowski P., Kornet S., Kowalczyk T., Banaś K., Bryk M., Ziółkowski P. J., Stajnke M., *Enhanced energy conversion as a result of fluid-solid interaction in micro- and nanoscale*, Journal Of Theoretical And Applied Mechanics **56**, 329–332, 2018.

[8] Badur J., Ziółkowski P., Kornet S., Stajnke M., Bryk M., Banaś K., Ziółkowski P. J., *The effort of the steam turbine caused by a flood wave load*, AIP Conference Proceedings **1822**, 2017.

[9] Badur J., Ziółkowski P., Zakrzewski W., Sławiński D., Banszkiewicz M., Kaczmarczyk O., Kornet S., Kowalczyk T., Ziółkowski P. J. *On the surface vis impressa caused by a fluid-solid contact,* Shell Structures: Theory and Applications Vol. **3**, 53–57, 2014.

[10] Badur J., Ziółkowski P., Zakrzewski W., Sławiński D., Kornet S., Kowalczyk T., Hernet J., Piotrowski R., Felicjancik J. and Ziółkowski P.J., *An advanced Thermal-FSI approach to flow heating/cooling,* Journal of Physics: Conference Series **530**, 2014.

[11] Banaś K., Badur J., *Influence of strength differential effect on material effort of a turbine guide vane based on thermoelastoplastic analysis,* Journal of Thermal Stresses **40**, 1368–1385, 2017.

[12] Bathe K. J., *Finite element procedures.* Englewood Cliffs, N.J., London 1996.

[13] Bilicki Z., Badur J., *A Thermodynamically consistent relaxation model for turbulent, binary mixture undergoing phase Transition.* Journal of Non-Equilibrum Thermodynamics **28**, 1–30, 2003.

[14] Dudda W., *Numerical analysis of a structure subject to corrosion degradation.* Bulletin of the IFFM No. 537/1496 (in Polish), Gdańsk 2005.

[15] Felicjancik J., Ziółkowski P., Badur J., *An advanced thermal-FSI approach of an evaporation of air heat pump.* Transactions of IFFM **129**, 111–141, 2015.

[16] Kornet S., Badur J., *Non-equilibrium phase transitions.* Logistyka 4 (in Polish), 225–233, 2013.

[17] McMeeking R. M., Rice J. R., *Finite-Element Formulations for Problems of Large Elastic-Plastic Deformation*, Internationa Journal of Solids and Structures **11** (5), 601–616, 1975.

[18] Sławiński D., *Start–up and shut–down steam turbine with used elasto–plastic material adaptation*, PhD thesis, IFFM PAS, Gdańsk 2015.

[19] Zakrzewski W., *Validation of the wet steam model by comparison with the experiment*, Modern technologies and energy conversion, Publisher Mechanical Department (in Polish), Gdańsk 2011.

[20] Zakrzewski W., Karcz M., Kornet S., *Estimation of the steam condensation flow via CFD methods*, Transactions of IFFM **124**, 111–124, 2012.